Cold sintering and electrical characterization of lead zirconate titanate piezoelectric ceramics

Dixiong Wang, Hanzheng Guo, Carl S. Morandi, Clive A. Randall, and Susan Trolier-McKinstry
Department of Materials Science and Engineering and Center for Dielectrics and Piezoelectrics, Materials Research Institute, The Pennsylvania State University, University Park, Pennsylvania 16802, USA

(Received 12 September 2017; accepted 5 December 2017; published online 2 January 2018)

This paper describes a cold sintering process for $Pb(Zr,Ti)O_3$ ceramics and the associated processing-property relations. $Pb(Zr,Ti)O_3$ has a very small, incongruent solubility that is a challenge during cold sintering. To circumvent this, a $Pb(NO_3)_2$ solution was used as the transient liquid phase. A bimodal lead zirconate titanate powder was densified to a relative density of 89% by cold sintering at 300 °C and 500 MPa. After the cold sintering step, the permittivity was 200, and the dielectric loss was 2.0%. A second heat-treatment involving a 3 h anneal at 900 °C increased the relative density to 99%; the resulting relative dielectric permittivity was 1300 at room temperature and 100 kHz. The samples showed well-defined ferroelectric hysteresis loops, having a remanent polarization of 28 $\mu C/cm^2$. On poling, the piezoelectric coefficient d_{33} was ~200 pC/N. With a 700 °C 3 h post-annealing, samples show a lower room temperature relative permittivity (950 at 100 kHz), but a 24 h hold time at 700 °C produces ceramics where there is an improved relative dielectric constant (1050 at 100 kHz). https://doi.org/10.1063/1.5004420

Lead Zirconate Titanate (PZT) piezoelectric ceramics are widely employed in ultrasound transducers,[1] precise positioning actuators,[2] sensors, and energy harvesters.[3] However typically PZT requires a sintering temperature >1200 °C.[4] Therefore, a number of methods have been explored to reduce the maximum processing temperature of PZT to 700 °C-1000 °C, including hot pressing,[5,6] liquid phase sintering,[7–9] microwave sintering,[10] and field assisted sintering (spark plasma sintering).[11]

The cold sintering process (CSP) can be used to reduce the processing temperature significantly by enabling the densification of ceramics at ultralow temperatures (<300 °C) under uniaxial pressure in the presence of a transient liquid phase. During this process, materials experience either congruent dissolution (Li_2MoO_4,[12] KH_2PO_4,[13] $NaNO_2$,[13] ZnO,[14] ZrO_2,[15] etc.) or incongruent dissolution ($BaTiO_3$[13,16,17]) in the liquid phase. Congruent dissolution favors rapid densification via cold sintering but is not always available in solids with complex chemistries. For example, in the case of $BaTiO_3$, the use of water as a liquid phase promotes leaching of Ba^{2+} with subsequent formation of $BaCO_3$ and passivation of the powder surfaces with an unreactive hydrated titanium-rich surface layer that prevents densification.[18] Thus, to avoid incongruent dissolution of $BaTiO_3$, a water based suspension of $Ba(OH)_2$ and TiO_2 can be utilized during cold sintering.[16,17] A challenge with the $BaTiO_3$ system was the fact that CO_2 stabilized an amorphous phase that fills the pores between the crystalline particles. This kinetically limited the sintering process until the carbonate is decomposed at a temperature of ~830 °C. Therefore a post-annealing stage was required to further densify and equilibrate the grain structures. A post-annealing at 900 °C produced high quality $BaTiO_3$ at a net reduction in temperature of 300-500 °C, relative to conventional methods.[13] The result is well-densified ceramics with high dielectric performance.

The objective of this paper is to consider another important perovskite ferroelectric material, $Pb(Zr,Ti)O_3$, and assess its feasibility with respect to the cold sintering process. On one hand, a lower

sintering temperature reduces the amount of lead loss, which may decrease the number of point defects in PZT (which could potentially improve the performance), but also leads to less pollution. For a multilayer actuator, the lower sintering temperatures could also be useful in broadening the range of metals that could be used for the inner electrodes. Given the importance of $Pb(Zr,Ti)O_3$ for pyroelectric or piezoelectric ceramics, it is also important to consider the high field properties, especially the ability to align the polarization under a poling process.[18]

In this work, a $Pb(NO_3)_2$ solution was used as a transient liquid sintering aid to densify the PZT powder. This solution was selected for 4 reasons: its high solubility in water, its low reactivity with CO_2 (limiting carbonate secondary phases), its compensation for lead loss during post-annealing, and its ability to act as a liquid phase sintering aid during post-annealing, if there is an excess of PbO after the cold sintering step. A 0.5 mol/l $Pb(NO_3)_2$ solution was made by dissolving 5.02 g $Pb(NO_3)_2$ (Sigma-Aldrich Corp., St. Louis, USA) into 30 ml de-ionized water.

A bimodal PZT powder was utilized for cold sintering PZT as this leads to a higher driving force for sintering and also can aid in the packing density. The coarse PZT powder is a commercial PZT-5A powder (PKI-509, Piezo Kinetics, Inc., Bellefonte, PA). To reduce the average particle size of ~3 μm, the powder was attrition milled (Szegvari Attritor System Type B Model 01-HD, Union Process, Inc., Akron, OH) to an average diameter ~400 nm. For the attrition milling, 25 vol. % PZT powder was suspended in de-ionized water with 3 vol. % Darvan A-21 dispersant (Vanderbilt Minerals, LLC, Norwalk, CT). The pH of the suspension was adjusted to ~10 with NH_4OH. The mixture was milled for 12 h, dried at 200 °C, and heat treated at 500 °C for 5 h to remove any residual carbon. The finer powder (undoped PZT 52/48) was made through a 2-methoxyethanol (2-MOE) based sol-gel method as described elsewhere.[19,20] Lead acetate trihydrate (Sigma-Aldrich) was added to 2-MOE in a rotary evaporator flask under Ar flow, dissolved at 120 °C, and distilled until a semi-dry powder precipitated. Zirconium n-propoxide (Sigma-Aldrich) and titanium iso-propoxide (Sigma-Aldrich) were mixed in 2-MOE at room temperature and then were added to the lead acetate. The mixture was refluxed for 3 h and distilled. Acetylacetone (22.5 vol. %, Sigma-Aldrich) and 2-MOE (Sigma-Aldrich) were added to make a 0.4 M solution. The solution was dried by stirring in air on a hot plate at 120 °C until a gel formed. The gel was crushed in an agate mortar and pestle and calcined at 600 °C for 42 h to remove the residual carbon from the precursors. The average diameter of the finer powder is ~100 nm.

To cold sinter PZT, 0.7 g of PZT bimodal powder (1:1 mixture of 400 nm and 100 nm powders in terms of weight) was mixed with 0.5 ml lead nitrate solution and ground in a mortar and pestle. The mixture was then loaded into a cylindrical die (Wartburg Tool & Die, Inc., Wartburg, TN) and pressed at 500 MPa uniaxial pressure (MP40 pellet press, Across International, LLC, Livingston, NJ). The die was held at room temperature for 30 min, heated to 300 °C for 150 min, and cooled down to <80 °C in 30 min. The PZT pellets after cold sintering had a diameter of 0.5 in. (12.77 mm) and thicknesses ~0.8-1.0 mm. Some of the cold sintered PZT pellets underwent a post-annealing step at 700 °C for 3 h, 700 °C for 24 h, or 900 °C for 3 h. The heating rate was 5 °C/min for all samples during the post-annealing process. To compare with the cold sintering process, in a conventional method, 0.7 g bimodal PZT powder was uniaxially pressed to a pellet under the same condition as that of CSP samples but without the addition of $Pb(NO_3)_2$ solution. The conventionally pressed pellet was also annealed 900 °C for 3 h which is the same as the CSP sample.

For grain size measurement, the PZT samples were polished using 15 μm, 9 μm, 6 μm, 3 μm, and 1 μm diamond polish, successively. Each step lasted for 2 min at a rotation speed of 240 rpm. The average grain size of the PZT samples was calculated by the line intercept method using the following equation:[21]

$$Average\ grain\ size = 1.5 \times \frac{total\ line\ length}{number\ of\ grain\ boundaries}.$$

The crystal structure and phase purity of the PZT samples were identified by X-ray diffraction (XRD, Empyrean, PANalytical Corp., Almelo, The Netherlands) with Cu Kα radiation. Scans were taken from $2\theta = 10°$ to 72° with a step size of 0.026° 2θ and a scan rate of 0.067°/s. A scanning electron microscope (SEM, Merlin, Carl Zeiss, Inc., Jena, Germany) and a transmission electron microscope (TEM, FEI Talos, Eindhoven, The Netherlands) with an energy dispersion spectroscope

TABLE I. The densities and d_{33} of the cold sintered PZT with different post-annealing temperatures. The d_{33} values are the average of 3 measurements of the same sample for each condition.

PZT samples (%)	Geometric density (g/cm^3)	Relative density (%)	Dielectric constant (100 kHz, 25 °C)	Loss (%)	d_{33} (pC/N)
Green compact 300 °C pressed	4.6	59	...	...	...
CSP 300 °C as sintered	6.9	89	207	2.0	4
CSP 700 °C 3 h post-annealed	7.1	91	917	2.7	80
CSP 900 °C 3 h post-annealed	7.7	99	1324	4.0	197

(EDS) detector were utilized to observe the microstructural development of the ceramics. After cutting, polishing, and focused ion beam milling the samples to electron transparency, they were mounted on copper grids.

The piezoelectric coefficients were measured by a direct method with a d_{33} PiezoMeter system (PM 300, Piezotest Pte. Ltd., Singapore) after a poling process at 25 °C for an hour under 3 times the coercive field. The polarization-electrical hysteresis loops (P-E loops) were characterized using a custom system with a Trek Model 30/20 high voltage amplifier system (Trek, Inc., Lockport, NY) and LabVIEW software (National Instruments Corporation, Austin, TX). The dielectric permittivity and loss tangent were measured using a Hewlett-Packard 4284A LCR meter (Agilent Technologies, Inc., Palo Alto, CA) over a temperature range from 500 °C to 30 °C.

Table I shows the geometric densities of PZT pellets heat treated at different temperatures. Using a theoretical density of 7.8 g/cm^3, the green compact sample [pressed without the $Pb(NO_3)_2$ sintering aid] yields a relative density of 59%. Cold sintering at 300 °C increases the relative density to 89%; after post-annealing at 900 °C, the relative density increases to 99%.

Figure 1 shows the XRD patterns after cold sintering and post-annealing. Crystalline $Pb(NO_3)_2$ and PbO are present after the cold-sintering step. In contrast, after the post-annealing step at higher temperatures, the samples are XRD phase pure, as $Pb(NO_3)_2$ decomposes and PbO volatilizes. It is probable that the relative densities of ceramics immediately following the cold sintering step and after a 700 °C post-annealing are similar due to the loss of this mass. After the 700 °C post-anneal, although the samples are XRD phase pure, there are clues that residual lead oxides may remain. This is inferred because even after the top and bottom surfaces were polished, orange stains were still seen on the sectioned surface of the pellet.

The microstructural evolution was investigated further using TEM with diffraction contrast imaging techniques. Upon cold-sintering at 300 °C, a dense structure forms due to consolidation of particles, and the grain boundaries have thick layers of amorphous and semi-glassy phases. This lead-rich matrix fills the spaces between the crystalline PZT particles. Nanocrystalline PbO or $Pb(NO_3)_2$,

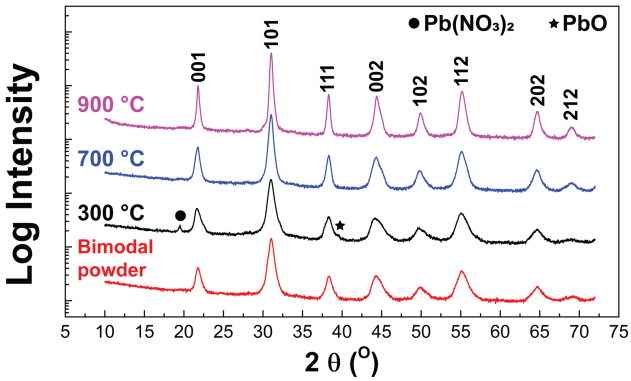

FIG. 1. XRD of the bimodal PZT powder, cold sintered at 300 °C as sintered PZT sample, and the samples after a 3 h post-annealing step. The spectra are offset vertically for clarity.

and amorphous phases form at the surface of the large PZT particles, presumably due to heterogeneous nucleation. Therefore, a primary benefit of cold-sintering is a major densification to a relative density of ~90%, and there is a reduction in distance between PZT particles and hence diffusion lengths. Upon post-annealing at 700 °C, well-defined grain boundaries and equilibrated triple points started to form, with dihedral angles ~120°. When the temperature increases to 900 °C, the melting of PbO increases mass transport, bringing the densification to completion. Within the grains, complex high-density domain configurations are formed [Figs. 2(f), 2(j), and 2(k)]. As for compositions, the EDS results presented in Figs. S1–S3 of the supplementary material indicate low carbon concentrations in cold sintered PZT although some zirconia impurities [Fig. S1(c) of the supplementary material] possibly from the commercial powder were observed.

Piezoelectric coefficients (d_{33}) of the cold sintered PZT are listed in Table I as well. The 900 °C annealed PZT has the highest d_{33} ~ 200 pC/N. This value is lower than that of commercial PZT-5A (350-550 pC/N) probably because the addition of 50 wt. % undoped PZT and the nanograin size.[6] It nonetheless demonstrates that it is possible to cold sinter PZT while retaining the functional

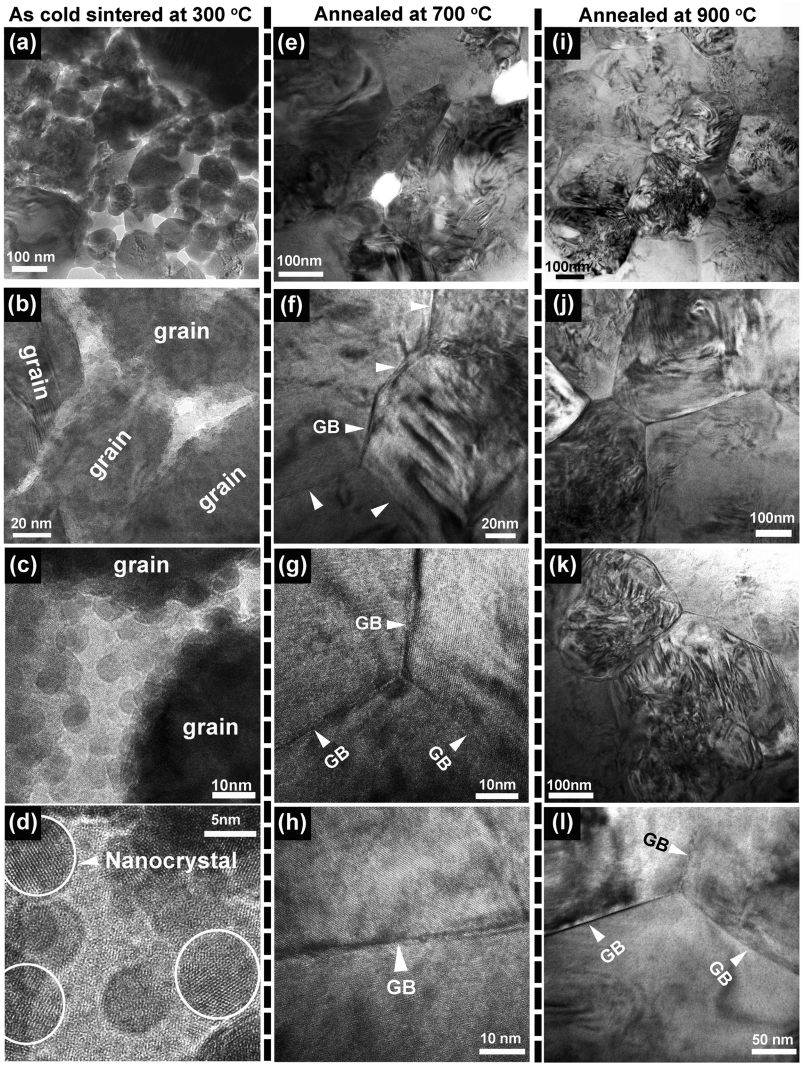

FIG. 2. Representative TEM bright-field micrographs of the microstructural evolution of PZT ceramics after [(a)–(d)] cold sintering at 300 °C, [(e)–(h)] annealing at 700 °C, and [(i)–(l)] annealing at 900 °C. Images with different magnifications are shown for each case to demonstrate the overall configuration and the regional characteristics around grain boundaries. Grain boundaries (GB) have been marked by the bright triangles.

properties, although at this point a post-annealing step is required to remove the grain boundary phases, and obtain a better density. The 700 °C annealed sample has a modest d_{33} most likely due to the presence of porosity, defects, and residual lead oxides. For the 300 °C cold sintered sample, almost no piezoelectric behavior can be detected.

In Fig. 3, the P-E loops and the permittivity-loss vs temperature curves of the PZT samples processed at different conditions are compared. It is clear that CSP PZT that has been post-annealed at 900 °C for 3 h has well-saturated P-E loops with higher remanent polarization and lower coercive field than the PZT pressed without cold sintering with $Pb(NO_3)_2$ [Fig. 3(a)]. Moreover [Fig. 3(c)], the dielectric permittivity of the 900 °C annealed CSP PZT is significantly higher than that of 900 °C annealed PZT without the cold sintering step (~1380 vs. ~650 at room temperature). This is most likely to be due to the pores in the conventionally processed PZT (Fig. S4 of the supplementary material) as it only has a geometric density ~75% after 900 °C annealing. The slightly higher dielectric loss in the CSP PZT annealed at 900 °C is likely to be a consequence of domain wall motion (the lower loss tangent at elevated temperatures suggests that the space charge contribution to the loss tangent is reduced in the cold sintered specimens).[18]

The TEM data also suggest the possibility for reducing the maximum process temperature of bulk PZT based on the closed triple point junctions. It was hypothesized that post-annealing at 700 °C for longer times may further improve the densification and yield better properties. Attempting to verify this hypothesis, a 24 h post-annealing procedure was utilized. The sample has a similar

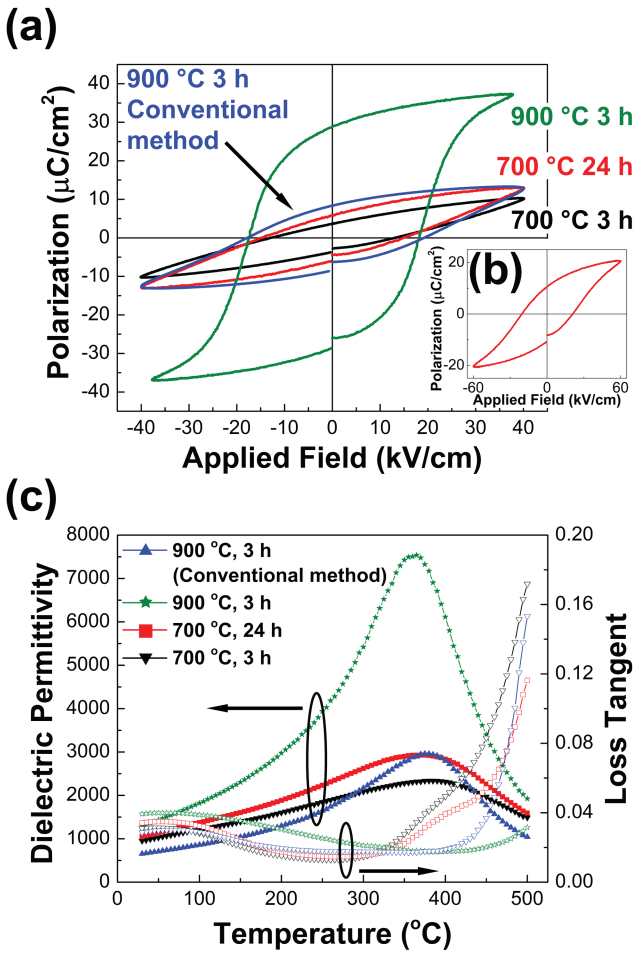

FIG. 3. (a) The P-E hysteresis loops of PZT post-annealed at 700 °C for 3 h and 24 h and at 900 °C for 3 h. The samples were measured under 10 Hz. (b) The P-E loop of 700 °C 24 h annealed PZT with higher maximum applied field (60 kV/cm) at 10 Hz. (c) The permittivity and loss of the post-annealed PZT at different temperatures under 100 kHz.

P-E hysteresis loop as the 3-h annealed sample when measured to maximum fields of 40 kV/cm [Fig. 3(a)]. On increasing the maximum field to 60 kV/cm, the polarization hysteresis loop begins to saturate and shows a remanent polarization of 10 μC/cm^2 [Fig. 3(b)]. Furthermore, the longer anneal at 700 °C produces a higher relative density (~93%) and dielectric permittivity, as indicated by Fig. 3(c). In addition, the long-time annealed PZT has a lower dielectric loss when the sample was heated to >350 °C, suggesting the reduction of excess PbO on increasing the annealing time.

Figure 4 compares the microstructure of the cold sintered ceramics with different second step annealing times. The 700 °C 3 h annealed PZT has an average grain size ~180 nm, while the 700 °C 24 h annealed PZT has an average grain size ~340 nm. Increasing the annealing time at 700 °C from 3 h to 24 h results in a larger grain size. In addition, the crystals in the 24-h annealed sample have polyhedral shapes, which is an indication of the final stage of sintering.

The experiments on long-time annealing indicate that since nanograined powders have a high surface energy that facilitates diffusion at lower temperatures, this helps further reduce the sintering temperature for PZT. Using the cold sintering procedure as a pre-treatment of the PZT powder, bulk PZT can possibly be sintered at as low as 700 °C. In the ceramic phase since grain boundaries act as pinning points, the piezoelectric properties will be somewhat degraded by the fine grain size. Further work is needed to reduce the thickness of the as-cold sintered grain boundary layers to minimize the reduction in functional properties.

In conclusion, PZT ceramics were cold sintered using bimodal PZT powder with $Pb(NO_3)_2$ as a sintering aid. Although the powder selection and the processing parameters need further optimization, early stage research achieved a relative density of ~90% at 300 °C by cold sintering. A post-annealing process through a post-annealing procedure at 900 °C for 3 h, which is 300-400 °C lower than conventional methods, is needed to develop good ferroelectric properties. In addition, 700 °C annealing also indicated promising densification for longer annealing times. The post-annealing step not only shows densification improvement, and equilibration of a nanosized grain structure, but also it produces ceramics with high relative permittivity, well-developed polarization switching with high remanent polarizations, and strong piezoelectric coefficients.

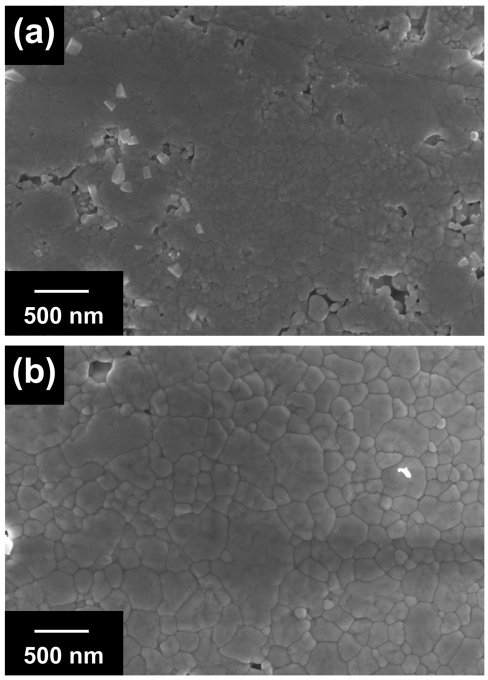

FIG. 4. Cross-sectional FESEM images of (a) cold sintered PZT ceramic annealed at 700 °C for 3 h. (b) Cold sintered PZT ceramic annealed at 700 °C for 24 h, with nanograin structures.

See supplementary material for the EDS data of the cold sintered PZT with different post-annealing temperatures. The fracture surface SEM images comparison between 900 °C post-annealed CSP PZT and 900 °C sintered PZT green compact.

The authors gratefully acknowledge financial support from the Steward S. Flaschen Professorship and the Air Force Office of Scientific Research. The material is also based upon work supported by the National Science Foundation, as part of the Center for Dielectrics and Piezoelectrics under Grant Nos. IIP-1361571 and 1361503. Meanwhile, the authors appreciate the help of Beth Jones and Amanda Baker on the preparation of PZT powders and the setup of cold sintering equipment.

[1] Z. Wang, Q.-T. Xue, Y.-Q. Chen, Y. Shu, H. Tian, Y. Yang, D. Xie, J.-W. Luo, and T.-L. Ren, Sensors **15**, 2538 (2015).
[2] Y. Miyahara, M. Deschler, T. Fujii, S. Watanabe, and H. Bleuler, Appl. Surf. Sci. **188**, 450 (2002).
[3] H. G. Yeo, X. Ma, C. Rahn, and S. Trolier-McKinstry, Adv. Funct. Mater. **26**, 5940 (2016).
[4] S. H. Cho and J. V. Biggers, J. Am. Ceram. Soc. **66**, 743 (1983).
[5] G. H. Haertling, J. Am. Ceram. Soc. **49**, 113 (1966).
[6] C. A. Randall, N. Kim, J.-P. Kucera, W. Cao, and T. R. Shrout, J. Am. Ceram. Soc. **81**, 677 (2005).
[7] R. B. Atkin and R. M. Fulrath, J. Am. Ceram. Soc. **54**, 265 (1971).
[8] T. Hayashi, T. Inoue, Y. Nagashima, J. Tomizawa, and Y. Akiyama, Ferroelectrics **258**, 53 (2001).
[9] T. Hayashi, T. Inoue, and Y. Akiyama, J. Eur. Ceram. Soc. **19**, 999 (1999).
[10] P. K. Sharma, Z. Ounaies, V. V. Varadan, and V. K. Varadan, Smart Mater. Struct. **10**, 878 (2001).
[11] Y. J. Wu, J. Li, R. Kimura, N. Uekawa, and K. Kakegawa, J. Am. Ceram. Soc. **88**, 3327 (2005).
[12] H. Kahari, M. Teirikangas, J. Juuti, and H. Jantunen, J. Am. Ceram. Soc. **97**, 3378 (2014).
[13] H. Guo, A. Baker, J. Guo, C. A. Randall, and D. Johnson, J. Am. Ceram. Soc. **99**, 3489 (2016).
[14] S. Funahashi, J. Guo, H. Guo, K. Wang, A. L. Baker, K. Shiratsuyu, and C. A. Randall, J. Am. Ceram. Soc. **100**, 546 (2017).
[15] H. Guo, T. J. M. Bayer, J. Guo, A. Baker, and C. A. Randall, Scr. Mater. **136**, 141 (2017).
[16] H. Guo, J. Guo, A. Baker, and C. A. Randall, ACS Appl. Mater. Interfaces **8**, 20909 (2016).
[17] H. Guo, A. Baker, J. Guo, and C. A. Randall, ACS Nano **10**, 10606 (2016).
[18] D. Damjanovic, Rep. Prog. Phys. **61**, 1267 (1998).
[19] R. A. Wolf and S. Trolier-McKinstry, J. Appl. Phys. **95**, 1397 (2004).
[20] K. D. Budd, S. Y. Dey, and D. A. Payne, Br. Ceram. Soc. Proc. **36**, 107 (1985).
[21] ASTM E112-13, ASTM Int. 1 (2013).